
CUT: A Controllable, Universal, and Training-Free Visual Anomaly Generation Framework

Han Sun¹, Yunkang Cao², Olga Fink³
^{1,3} EPFL ² HUST

Abstract

Visual anomaly detection (AD) inherently faces significant challenges due to the scarcity of anomalous data. Although numerous works have been proposed to synthesize anomalous samples, the generated samples often lack authenticity or can only reflect the distribution of the available training data samples. In this work, we propose **CUT**: a **C**ontrollable, **U**niversal and **T**raining-free visual anomaly generation framework, which leverages the capability of Stable Diffusion (SD) in image generation to generate diverse and realistic anomalies. With CUT, we achieve controllable and realistic anomaly generation universally across both unseen data and novel anomaly types, using a single model without acquiring additional training effort. To demonstrate the effectiveness of our approach, we propose a **V**sion-**L**anguage-based **A**nomaly **D**etection framework (VLAD). By training the VLAD model with our generated anomalous samples, we achieve state-of-the-art performance on several benchmark anomaly detection tasks, highlighting the significant improvements enabled by our synthetic data. Our project page: <https://hansunhayden.github.io/CUT.github.io/>

1 Introduction

Visual anomaly detection (AD) [1] is a crucial task in many fields, including quality control, industrial inspection [2], and medical diagnosis [3]. Since anomalies are rare and difficult to collect, most existing AD methods rely on unsupervised learning [4, 5, 6] using only normal samples. Despite recent advancements in the AD field, the scarcity of anomalous samples for training remains a persistent challenge.

To address this challenge, various studies have focused on visual anomaly generation, as illustrated in Figure 1. One approach [7, 8] augments normal samples by cropping and pasting random patterns, either from natural patterns in other datasets or the image itself. While this results in diverse anomalous samples, they often appear unrealistic. Another approach generates visual anomalies using generative models[9]. While those models produce more realistic images, they require sufficient and representative normal and/or abnormal samples for training, which is typically challenging for AD. Due to the infrequent occurrence and potential wide variety of anomalies, it is difficult to collect a sufficiently representative set of anomalous samples. Additionally, the diversity of product variants and configurations in industrial applications often results in a lack of representative normal samples, posing another significant challenge. The challenges result in a shortage of both abnormal and normal samples. Therefore, these generative models are often not applicable in real-world applications with data scarcity and tend to be biased towards the limited available observations used for training.

Given the limitations of existing visual anomaly generation methods, we aim to achieve realistic, diverse, while training-free anomaly generation. The goal inspires us to explore Stable Diffusion (SD) [10], which is a latent text-to-image diffusion model that has demonstrated considerable capabilities for generating diverse images across various domains. However, despite SD’s impressive image generation performance in many different applications, it is not specialized for visual anomaly

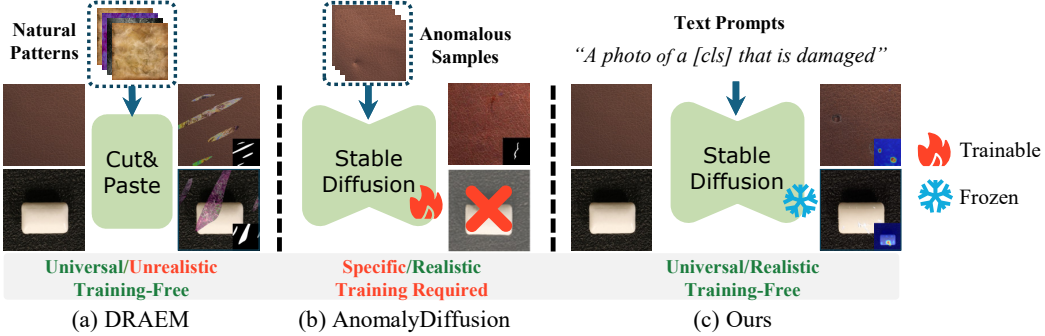


Figure 1: Comparison between existing visual anomaly generation methods and ours.

generation. As a result, when directly applied for anomaly generation, the images generated by SD may deviate from the desired normal distribution and fail to accurately represent realistic anomaly patterns. One proposed solution [8, 9], is to fine-tune SD on available normal/anomalous samples. However, this approach may undermine SD’s ability to generalize to unseen data and anomaly types.

In this work, we propose **CUT**: a **Controllable**, **Universal**, and **Training-free** visual anomaly generation framework. We leverage the pretrained SD model to generate anomalous patterns by providing text descriptions as input, which can include specific details of the desired anomaly type, such as ‘crack’ or ‘scratch’, offering **controllability** to the generation process. Instead of fine-tuning SD on available normal data, we introduce **training-free** normal distribution guidance by conditioning each generation process with a normal sample. This preserves the diversity and generalization ability of SD, enabling **universal** anomaly generation on unseen data and anomaly types. With this one model, we are able to generate realistic and diverse anomalous samples for any new objects and arbitrary anomaly descriptions. We observe that the original SD fails to generate realistic anomaly samples due to two inherent challenges: first, anomalies are comparatively rare in the training data for SD; second, unlike common objects and patterns, anomalous patterns typically occupy only a small region of the image, making them easy to be neglected in the generation result. Therefore, we introduce mask-guided attention optimization to guide the model’s attention on generating anomalies by maximizing the attention value correlated with the anomaly token. To further prevent unrealistic generation artifacts caused by over-optimization within a local region, we propose a localization-aware scheduler to adjust the optimization speed at each step based on the area of the activated anomaly region, coupled with an early stopping strategy. Additionally, we use the attention map related to the anomaly token as a coarse pixel-level annotation to localize the anomaly and further propose an adapted dice loss for robust training of downstream AD tasks under such weak supervision.

Furthermore, we develop a multi-class vision-language-based anomaly detection framework (VLAD). Instead of using real anomaly data, we train the VLAD with samples generated by CUT. The results show significantly better multi-class AD performance under both unsupervised and few-shot setups, demonstrating the effectiveness of CUT. Our main contributions can be summarized as follows:

- We propose CUT, a controllable, universal, and training-free visual anomaly generation framework for diverse and realistic anomaly generation. Users can provide arbitrary normal images and anomaly descriptions to generate corresponding realistic anomalous samples.
- We introduce mask-guided attention optimization along with a localization-aware optimization scheduler to overcome the limitations of SD in anomaly generation. Our proposed method achieves more authentic generation results compared to other existing methods, even without additional training.
- We propose a pipeline to generate abundant synthetic anomalous samples with image-level and coarse pixel-level annotations. We further propose an adapted version of dice loss for robust training of AD tasks with our anomaly image-annotation pairs.
- We validate the effectiveness of our generated anomalous samples in facilitating training the proposed VLAD model and achieved competitive AD performance on MVTec and VisA in multi-class unsupervised and few-shot AD tasks.

2 Related Works

2.1 Anomaly Detection

The scarcity of available anomalous samples has made **unsupervised anomaly detection** a dominant paradigm in the AD field. This approach aims to model the normal distribution and then identify anomalies as outliers. Most previous methods train separate models for different object categories to learn a compact normal distribution boundary per object [11, 12, 13]. Recently, multi-class unsupervised anomaly detection has emerged, aiming to detect anomalies across multiple categories using a single model [4, 5]. However, all the aforementioned methods assume the availability of a sufficient amount of normal samples that are adequately representative of the underlying distribution. Due to the shortage of representative normal samples from the wide range of variations in products and industrial configurations, multi-class **few-shot anomaly detection** has been gaining popularity. Existing few-shot methods typically leverage additional knowledge from vision-language models pretrained on large-scale datasets, such as Contrastive Language-Image Pre-training (CLIP) [14], to compute the similarity between data samples and the normal/abnormal text prompts [15, 16, 17]. Nevertheless, training AD models with solely normal samples remains challenging due to the lack of awareness of anomaly distributions, highlighting the need for realistic anomalous samples to enhance AD performance.

2.2 Anomaly Generation

The scarcity of anomalous data has motivated numerous studies to synthesize anomaly samples. One branch of methods augments normal training samples by cropping and pasting abnormal patterns from few-shot abnormal samples in the test set [18, 19], from natural patterns of external datasets [20, 7], or directly from the normal image itself [21, 22]. Despite being simple and effective, these methods lack authenticity and diversity of the generated samples. Another branch of methods uses generative models, such as generative adversarial networks (GANs) to synthesize anomaly samples [23, 24]. More recently, with advancements in diffusion models, [9, 25, 8] have leveraged the strong prior information of diffusion models and fine-tune them on anomaly data for more diverse and more realistic anomaly generation. However, these methods typically require access to substantial amounts of normal and/or abnormal data samples to learn the specific data distribution of the dataset at hand, which is impractical in data-limited scenarios. Diverging from these methods, CUT directly deploys the pretrained SD model for anomaly synthesis without additional training efforts, offering a more flexible solution for high-quality anomaly generation under setups of highly diverse objects and arbitrary domains.

3 Preliminary: Stable Diffusion

Diffusion models. Denoising diffusion probabilistic models (DDPMs) [26] learn the desired data distribution by defining a Markov chain of length T . In the forward pass, this chain gradually adds noise to a given data sample x_0 to obtain a sequence of noisy samples $x_t, t \in T$. In the reverse process, a model parameterized by θ is learned to predict the noise added for each step t . During inference, the reverse process starts with a random noise $x_T \sim \mathcal{N}(0, \mathbf{I})$ and gradually generates an image sample from the noise from step T to 0. Our method is based on SD [10], which applies the diffusion process in the latent space of a variational auto-encoder (VAE).

Text condition. SD introduces text guidance via a cross-attention mechanism. The denoising UNet network in the latent space of SD consists of self-attention layers followed by cross-attention layers at resolutions $P \in (64, 32, 16, 8)$. Given a text prompt c composed of N tokens, a guidance vector $\tau_\theta(c)$ is then obtained via the CLIP text-encoder τ_θ [27]. $\tau_\theta(c)$ is then mapped to intermediate feature maps of the DDPM model ϵ_θ through each cross-attention layer as follows:

$$A = \text{attn}(Q, K, V) = \text{softmax} \left(\frac{QK^T}{\sqrt{d}} \right) \cdot V, \quad A \in [P, P, N] \quad (1)$$

$$Q = W_Q^{(i)} \cdot \varphi_i(z_t), K = W_K^{(i)} \cdot \tau_\theta(y), V = W_V^{(i)} \cdot \tau_\theta(c) \quad (2)$$

where $\varphi_i(z_t)$ is the intermediate feature of the UNet. A, Q, K, V denote the attention, query, key, and value matrices, respectively. The $W^{(i)}$ terms are learnable projection matrices.

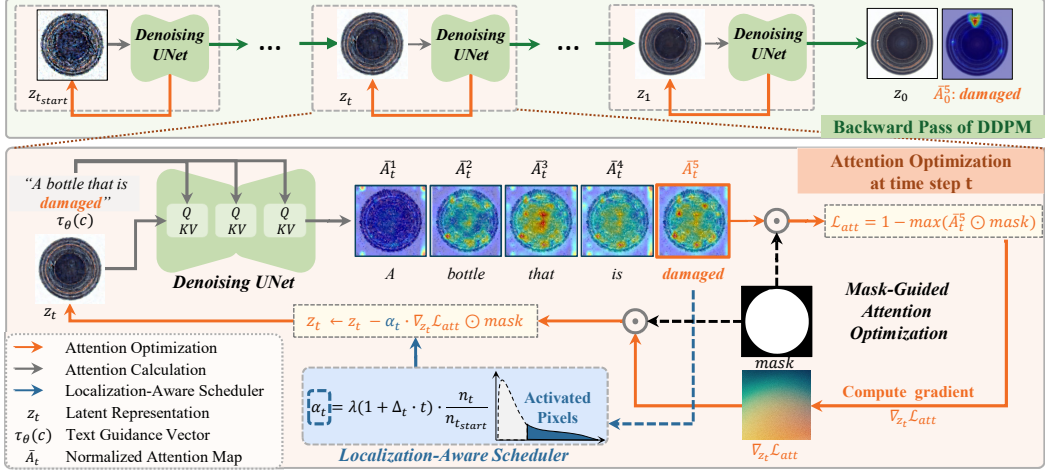


Figure 2: Illustration of CUT with details of the attention optimization process at time step t .

4 Methodology

In this work, we propose CUT for universal anomaly data generation on unseen objects and anomaly types, as shown in Figure 2. Considering the inherent nature of anomalies and the challenges in generating them, we propose a mask-guided optimization scheme with a localization-aware scheduler within this framework. This approach significantly improves the quality of anomaly generation, as detailed in Sec. 4.1. Furthermore, we develop VLAD, a multi-class anomaly detection framework, and train it on our generated samples for enhanced anomaly detection performance, as introduced in Sec. 4.2.

4.1 Controllable, Universal and Training-free Visual Anomaly Generation Framework

Training-free normal distribution conditioning via normal samples. CUT leverages SD to generate visual anomalies. While SD is effective in image generation, the inherent diversity in SD’s underlying distribution causes the generated images to differ significantly from the normal images in a specific AD dataset, as shown in Figure 3(b). To generate images that adhere to the desired normal distribution, we directly leverage information from normal samples during the generation process. Given a normal sample x^{normal} and its latent representation $z^{normal} = \mathcal{E}(x^{normal})$ encoded by the VAE encoder, we get a sequence of samples $z_1^{normal}, z_2^{normal}, \dots, z_T^{normal}$ with increasingly added noise controlled by the DDPM noise scheduler. Instead of starting the inference from $z_T \sim \mathcal{N}(\mathbf{0}, \mathbf{I})$, we start from step $t_{start} = T \cdot (1 - \gamma)$ with the noisy latent representation $z_{t_{start}}^{normal}$, which conveys corrupted features from the guidance normal image x^{normal} . The parameter γ controls the starting step, i.e., the noise scale added to the guidance data sample. In our experiments, we set $\gamma = 0.25$ to balance similarity to the original distribution and inference steps for diverse results.

Controllable anomaly generation via text description. We generate anomalous samples of a specific object type, denoted as $[cls]$ (e.g., bottle), by providing anomaly text descriptions, such as "A photo of a $[cls]$ that is damaged". Anomaly generation presents unique challenges distinct from other image generation tasks. Firstly, anomaly descriptions involve rare concepts that are challenging for the SD model. Secondly, anomalies typically occupy only a small region of the image and are not the primary focus, making it difficult for SD to focus on these areas. As a result, the desired anomaly semantics are often neglected in the generated images, as shown in Figure 3(d). To overcome these challenges, we introduce **mask-guided attention optimization** to enforce the generation of the critical but challenging concepts of anomalies. First, we aggregate the attention maps from SD for later optimization. As introduced in Sec. 3, SD introduces text guidance based on the cross-attention mechanism. Given a text prompt c with N tokens, for each pass at step t during the inference process, we obtain a collection of attention maps $A_t \in P \times P \times N$ with respect to c at different resolutions. These attention maps represent the cross-correlation with each text token, i.e., $A[:, :, i]$ denotes the probability assigned to token $c_i, i \in (1, N)$. Referring to [28], we average all the attention maps

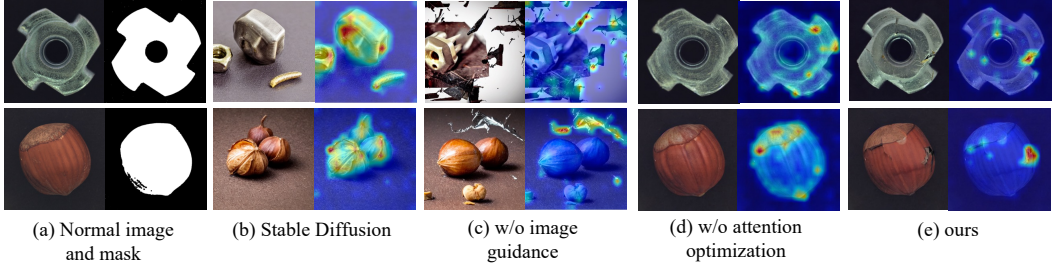


Figure 3: Examples of generated anomaly samples and attention map of *damage*. We present (a) Normal guidance image and foreground mask, and the results generated by (b) Stable Diffusion, (c) ours w/o image guidance, (d) ours w/o attention optimization, and (e) our proposed method.

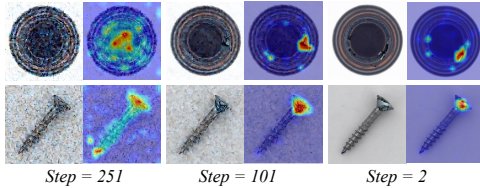


Figure 4: Visualization of intermediate generation results and the attention maps at different denoising steps.

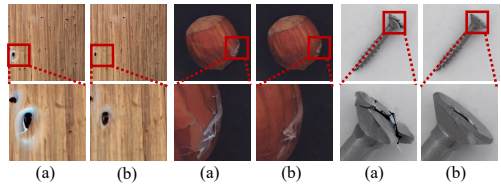


Figure 5: Examples of anomalies generated by our method (a) w/o; (b) w/ localization-aware scheduler & the early stopping strategy.

with a resolution of 16×16 , which are shown to be the most semantically informative ones. The resulting attention map \bar{A}_t is normalized along the dimension of tokens and then smoothed with a $\text{Gaussian}(\cdot)$ function:

$$\bar{A}_t = \text{Gaussian}(\text{softmax}(\bar{A}_t)), \quad \bar{A}_t \in 16 \times 16 \times N \quad (3)$$

Our goal is to enforce the generated image to convey the semantic meaning of the anomaly type token c_j from the given c , e.g., "damaged" in "A photo of a [cls] that is damaged". During the generation process, at each time step t , we optimize the intermediate latent representation z_t by maximizing the attention related to the anomaly description. The optimized latent representation is denoised to obtain z_{t-1} for the next optimization and denoising step, as shown in Figure 2. Specifically, for optimization at step t , we extract the attention map $\bar{A}_t^j = \bar{A}_t[:, :, j]$ correlated with the anomaly token c_j , and then obtain the update gradient of z_t with respect to the loss function \mathcal{L}_{att} computed on \bar{A}_t^j . To constrain the generated anomaly on the object, we only compute the loss and optimize z_t within the foreground mask region. We formulate the optimization at step t as:

$$\mathcal{L}_{att} = 1 - \max \left(\bar{A}_t^j \odot \text{mask} \right), \quad z_t \leftarrow z_t - \alpha_t \cdot \nabla_{z_t} \mathcal{L}_{att} \odot \text{mask} \quad (4)$$

where α_t is a scalar defining the step size. The foreground mask is obtained with simple binary thresholding. The optimization objective encourages a large maximum value of \bar{A}_t^j to strengthen the activations of the anomaly token. To ensure a large enough attention for the anomaly token, at each time step, we repeat the optimization several times until the value of $\max(\bar{A}_t^j \odot \text{mask})$ is above a pre-defined threshold. With this step-by-step optimization, we ensure that the anomaly semantics are progressively incorporated into the generated image, as illustrated in Figure 4.

Our empirical findings indicate that the above iterative update can lead to redundant attention and introduce artifacts into the image. As shown in Figure 4, the attention map becomes localized and activated in the early steps already. Over-optimization within this small region can significantly distort the data distribution, resulting in unrealistic patterns. To mitigate this issue, we propose a **localization-aware scheduler combined with an early-stopping strategy**. Given the initial generation result $z_{t_{start}}$ and its attention map $\bar{A}_{t_{start}}^j$, we calculate the number of activated pixels $n_{t_{start}}$ with values above the mean in the smoothed attention map. At each step, we compute the scalar α_t as follows:

$$\alpha_t = \lambda(1 + \Delta_t \cdot t) \cdot \frac{n_t}{n_{t_{start}}} \quad (5)$$

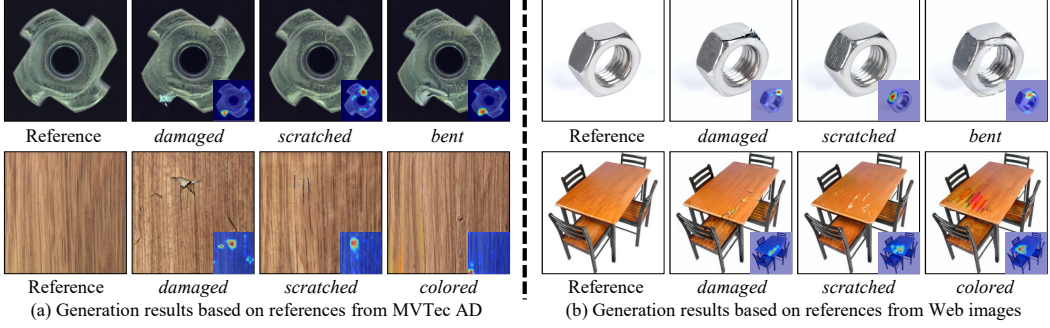


Figure 6: Anomaly generation results for arbitrary objects and anomaly descriptions. The bottom right presents the generated coarse pixel-level annotations.

where λ is a scale factor to control the optimization strength, and Δt controls the step size to gradually decrease the update speed. n_t denotes the number of activated pixels above the mean at time step t . As the attention gradually focuses more on a smaller region dominated by fewer high-value pixels, we consider the attention to be more optimized and localized. Accordingly, we decrease α_t to avoid overfitting. When the number of activated pixels n_t falls below a certain threshold, we apply early stopping and proceed with the remaining denoising steps without the attention-based optimization. As shown in Figure 5, this proposed strategy greatly reduces unrealistic artifacts in the generated samples.

With our proposed CUT approach, we achieve controllable and training-free anomaly generation. Notably, since CUT is not trained on any specific datasets, it is not limited by the distribution of available normal samples and can be applied universally to a wide range of unseen object categories and anomaly types. Additionally, the attention maps define a probability distribution over each text token, allowing us to use the final smoothed attention map \bar{A}_0^j at time step 0 as a coarse pixel-level annotation to localize the anomaly described by c_j . Formally, given a normal image x^{normal} , each generation process yields a corresponding realistic anomalous sample x along with its binary image-level and probability-aware pixel-level annotations (y_{img}, y_{pix}) conditioned on a text prompt c that describes desired anomaly types. Due to the inherent randomness in the denoising process, multiple passes of CUT result in a dataset of diverse anomalous image-annotation pairs, which we use for training downstream AD tasks, as described in Sec. 4.2.

4.2 Vision-Language-based Anomaly Detection

To evaluate the effectiveness of our proposed method, we introduce VLAD and train it on the anomalous samples generated by CUT. The proposed VLAD is built on the competitive CLIP-based AD method [16], with an adapted training objective. Our training objective comprises two parts: an image-level classification loss and a pixel-level localization loss. For binary classification of normal and anomalous images, we employ focal loss [29] to emphasize the hard misclassified examples. For anomaly localization, we apply standard binary cross-entropy (BCE) loss combined with Dice loss [30] to address unbalanced segmentation training. Given the imprecision of our pixel labels, we introduce an adapted version of Dice loss to prevent the over-prediction of abnormal regions:

$$\text{Dice}(y_{pix}, \hat{y}_{pix}) = \frac{2 \cdot y_{pix} \cdot \hat{y}_{pix} + 1}{y_{pix} + \hat{y}_{pix} + 1}, \quad \mathcal{L}_{\text{Dice}} = 1 - \frac{\text{Dice}}{\text{Dice} + \beta} \quad (6)$$

where β is a scaling factor. A smaller β value reduces the adapted Dice loss compared to the original version when the prediction is imprecise but overlaps with the ground truth. This adjustment reduces the regularization, allowing for better fitting of the coarse annotation. Our overall training objective is formulated as:

$$\mathcal{L} = \mathcal{L}_{\text{focal}}(y_{img}, \hat{y}_{img}) + \omega(\mathcal{L}_{\text{BCE}}(y_{pix}, \hat{y}_{pix}) + \mathcal{L}_{\text{Dice}}(y_{pix}, \hat{y}_{pix})) \quad (7)$$

where ω is a weight factor used to balance the loss terms, set to 6.0 in all experiments. More details of VLAD are provided in Sec. A.2.

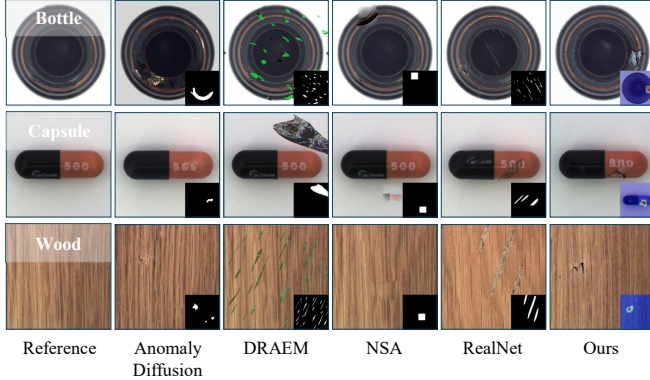


Figure 7: Qualitative comparisons between existing anomaly generation methods.

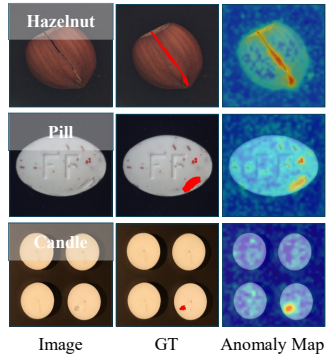


Figure 8: Anomaly detection results in the 4-shot setup.

5 Experiment

Our experiments are divided into two main parts: anomaly generation and anomaly detection. First, we evaluate the performance of CUT in generating anomalies, comparing it to other anomaly generation methods. Following this, we use the generated anomalous data to train our VLAD model. The VLAD model is then evaluated under various conditions, including multi-class few-shot (1, 2, 4-shot) and full-shot scenarios, to provide a comprehensive analysis of its performance.

5.1 Experimental Setup

Datasets & setups. We conduct extensive experiments on MVTec AD [31] and VisA [32]. For the different anomaly detection scenarios, we randomly select k normal samples from their training sets, where $k = 1, 2, 4$, all for the 1, 2, 4-shot and full-shot setups, respectively. We condition on the k selected normal images and generate $100k$ and $5k$ anomalous samples with corresponding annotations for the few-shot and full-shot tasks respectively. Then we use them to train VLAD. Under the general assumption in AD that anomaly types are unknown, we utilize a common text prompt "A photo of a [cls] that is damaged" for anomaly generation by default. Since few-shot anomaly detection performance is significantly influenced by the selected normal samples, we report the mean and standard deviation over five runs, while we only conduct a single run for the full-shot setup.

Evaluation metrics. For the anomaly detection task, we employ five metrics to thoroughly evaluate the detection performance. We evaluate the results with image-level and pixel-level Area Under the Receiver Operating Characteristic (AUROC), denoted as I-AUC and P-AUC, respectively. Additionally, we report the image-level and pixel-level max-F1 scores [15], denoted as I-F1 and P-F1, and Per-Region-Overlap [2] denoted as PRO.

Implementation details. For anomaly generation, we deploy the pretrained SD model¹. For anomaly detection, we construct the anomaly detection module with ViT-L/14² and train the model on the generated anomalous samples for 200 training epochs and a learning rate of 1e-4. During training, following [16], we use MVTec AD as auxiliary data for VisA and VisA as auxiliary data for MVTec AD. More implementation details are provided in Appendix Sec. A.1.

5.2 Anomaly Generation Results

Anomaly generation with arbitrary anomaly text descriptions and object types. Compared to data generation methods like [23, 9, 25], our method CUT requires no training on normal and/or anomalous samples. Thus, CUT is not constrained by the limited available training data distribution, presenting universal anomaly generation capabilities on unseen data and arbitrary anomaly types, as shown in Figure 6. We present more generation results in Figure 11 and Figure 12 in Appendix. This shows our method's great potential in personalized anomaly generation with arbitrary normal patterns

¹<https://huggingface.co/runwayml/stable-diffusion-v1-5>

²https://github.com/mlfoundations/open_clip

Table 1: Comparison of few-shot anomaly detection on MVTec AD and VisA. Results are reported over 5 runs. The best results are in **bold**, and the second-best results are underlined.

Setup	Methods	MVTec AD					VisA				
		I-AUC	I-F1	P-AUC	P-F1	PRO	I-AUC	I-F1	P-AUC	P-F1	PRO
1-shot	PaDiM	76.6 \pm 3.1	88.2 \pm 1.1	89.3 \pm 0.9	40.2 \pm 2.1	73.3 \pm 2.0	62.8 \pm 5.4	75.3 \pm 1.2	89.9 \pm 0.8	17.4 \pm 1.7	64.3 \pm 2.4
	PatchCore	83.4 \pm 3.0	90.5 \pm 1.5	92.0 \pm 1.0	50.4 \pm 2.1	79.7 \pm 2.0	79.9 \pm 2.9	81.7 \pm 1.6	95.4 \pm 0.6	38.0 \pm 1.9	80.5 \pm 2.5
	WinCLIP+	93.1 \pm 2.0	<u>93.7\pm1.1</u>	95.2 \pm 0.5	<u>55.9\pm2.7</u>	<u>87.1\pm1.2</u>	83.8 \pm 4.0	<u>83.1\pm1.7</u>	96.4 \pm 0.4	<u>41.3\pm2.3</u>	<u>85.1\pm2.1</u>
	AnomalyGPT	94.1 \pm 1.1	-	95.3 \pm 0.1	-	-	87.4 \pm 0.8	-	96.2 \pm 0.1	-	-
	PromptAD	94.6 \pm 1.7	-	95.9\pm0.5	-	-	86.9 \pm 2.3	-	96.7 \pm 0.4	-	-
2-shot	Ours	94.9\pm0.4	94.7\pm0.4	<u>95.4\pm0.2</u>	57.3\pm0.0	91.9\pm0.0	89.7\pm0.8	85.8\pm0.5	97.7\pm0.4	43.2\pm0.4	92.5\pm0.1
	PaDiM	78.9 \pm 3.1	89.2 \pm 1.1	91.3 \pm 0.7	43.7 \pm 1.5	78.2 \pm 1.8	67.4 \pm 5.1	75.7 \pm 1.8	92.0 \pm 0.7	21.1 \pm 2.4	70.1 \pm 2.6
	PatchCore	86.3 \pm 3.3	92.0 \pm 1.5	93.3 \pm 0.6	53.0 \pm 1.7	82.3 \pm 1.3	81.6 \pm 4.0	82.5 \pm 1.8	96.1 \pm 0.5	41.0 \pm 3.9	82.6 \pm 2.3
	WinCLIP+	94.4 \pm 1.3	<u>94.4\pm0.8</u>	96.0 \pm 0.3	<u>58.4\pm1.7</u>	<u>88.4\pm0.9</u>	84.6 \pm 2.4	<u>83.0\pm1.4</u>	96.8 \pm 0.3	<u>43.5\pm3.3</u>	<u>86.2\pm1.4</u>
	AnomalyGPT	95.5 \pm 0.8	-	95.6 \pm 0.2	-	-	88.6 \pm 0.7	-	96.4 \pm 0.1	-	-
4-shot	PromptAD	95.7 \pm 1.5	-	96.2\pm0.3	-	-	88.3 \pm 2.0	-	<u>97.1\pm0.3</u>	-	-
	Ours	95.8\pm0.2	95.2\pm0.2	96.0 \pm 0.2	58.8\pm0.2	92.6\pm0.1	91.3\pm0.4	87.2\pm0.6	97.9\pm0.4	44.9\pm0.3	92.7\pm0.1

Table 2: Comparison of full-shot anomaly detection on MVTec AD and VisA. The best results are in **bold**, and the second-best results are underlined.

Methods	MVTec AD					VisA				
	I-AUC	I-F1	P-AUC	P-F1	PRO	I-AUC	I-F1	P-AUC	P-F1	PRO
UniAD	96.5	<u>98.8</u>	96.8	43.4	90.7	88.8	<u>90.8</u>	98.3	33.7	85.5
SimpleNet	95.3	<u>98.4</u>	<u>96.9</u>	45.9	<u>86.5</u>	<u>87.2</u>	<u>87.0</u>	96.8	<u>34.7</u>	<u>81.4</u>
DiAD	97.2	99.0	96.8	<u>52.6</u>	<u>90.7</u>	86.8	88.3	96.0	26.1	75.2
AnomalyGPT	97.4	-	93.1	-	-	-	-	-	-	-
Ours	98.4	96.9	97.4	65.1	94.7	95.8	91.9	98.7	58.7	97.7

and anomalous descriptions, and may greatly contribute to the enhancement of anomaly detection models for a specific category even without real collected anomalous samples.

Comparison in anomaly generation with other methods. We compare CUT with several existing anomaly generation methods, including DRAEM [7], NSA [22], RealNet [8], and AnomalyDiffusion [9]. Among these methods, AnomalyDiffusion trains on anomalous data from the test set and may introduce data leakage. Figure 7 presents the generated anomalies of these methods. We include more examples in Figure 10 in Appendix. The examples clearly show that DRAEM, NSA, and RealNet introduce inauthentic patterns, while AnomalyDiffusion and CUT can generate more realistic anomalous samples. Notably, AnomalyDiffusion requires anomalous training data, while CUT is training-free and presents better generalization ability. A user study on anomaly generation quality is provided in Sec. A.3, further demonstrating the superior data generation quality of CUT. To admit, without training, CUT currently generates only coarse pixel-level annotations. We aim to enhance these annotations for greater precision in the future.

5.3 Anomaly Detection Results

Few-shot anomaly detection. Table 1 presents the comparison results between ours and existing few-shot AD methods, including two full-shot methods PaDiM [33], PatchCore [13] in the few-shot settings, and three CLIP-based few-shot methods WinCLIP+ [15], AnomalyGPT [16], and PromptAD [17]. As can be seen, VLAD trained with our generated anomalous samples consistently outperforms other alternatives in the majority of the metrics. In comparison to the second-place methods, ours achieves significant improvements, e.g., 2.3%, 2.7%, and 1.1% I-AUCs under the 1, 2, and 4-shot setups for VisA. Figure 8 visualizes the 4-shot detection result, presenting the precise localization ability of our trained VLAD model. We provide the per-category detection results in Table 6 to Table 11 and more visualizations of detection results in Figure 13 in Appendix.

Table 3: Comparisons between anomaly detection performance with different anomaly generation methods. Since AnomalyDiffusion utilizes anomalous data for training and results in data leakage, we exclude it from ranking. The best results are in **bold**, and the second-best results are underlined.

Methods	MVTec AD					VisA				
	I-AUC	I-F1	P-AUC	P-F1	PRO	I-AUC	I-F1	P-AUC	P-F1	PRO
AnomalyDiffusion	94.4 \pm 0.3	94.4 \pm 0.2	95.3 \pm 0.5	57.3 \pm 3.0	92.2 \pm 1.0	-	-	-	-	-
DRAEM	93.6 \pm 0.3	94.2 \pm 0.4	<u>95.1\pm0.1</u>	56.0 \pm 0.9	<u>91.8\pm0.1</u>	86.0 \pm 0.7	83.0 \pm 0.9	<u>97.5\pm0.1</u>	42.6 \pm 0.7	<u>92.6\pm0.6</u>
NSA	94.0 \pm 0.5	94.2 \pm 0.3	<u>95.1\pm0.1</u>	56.1 \pm 0.5	<u>91.8\pm0.2</u>	86.2 \pm 2.0	83.1 \pm 1.2	97.4 \pm 0.1	40.8 \pm 0.5	92.3 \pm 0.3
RealNet	92.7 \pm 0.7	93.6 \pm 0.3	<u>95.1\pm0.1</u>	56.3 \pm 1.3	91.7 \pm 0.1	86.0 \pm 1.4	82.9 \pm 1.1	<u>97.5\pm0.2</u>	41.9 \pm 1.8	<u>92.8\pm0.3</u>
Ours	94.9\pm0.4	94.7\pm0.4	<u>95.4\pm0.2</u>	<u>57.3\pm0.0</u>	91.9\pm0.0	<u>89.7\pm0.8</u>	<u>85.8\pm0.5</u>	<u>97.7\pm0.4</u>	43.2\pm0.4	92.5 \pm 0.1

Table 4: Ablations on image-level supervision and pixel-level coarse supervision.

Supervision	MVTec AD					VisA				
	I-AUC	I-F1	P-AUC	P-F1	PRO	I-AUC	I-F1	P-AUC	P-F1	PRO
y_{pix}	93.4 \pm 0.6	93.8 \pm 0.3	95.4\pm0.0	57.0 \pm 0.2	92.0\pm0.0	85.7 \pm 1.1	82.4 \pm 1.0	97.7\pm0.1	42.8 \pm 1.0	92.9\pm0.2
y_{img}	94.0 \pm 0.2	94.2 \pm 0.3	95.0 \pm 0.1	55.8 \pm 0.4	91.7 \pm 0.1	87.3 \pm 0.6	83.5 \pm 0.5	97.5 \pm 0.1	42.1 \pm 1.1	92.7 \pm 0.3
y_{img}, y_{pix}	94.9\pm0.4	94.7\pm0.4	<u>95.4\pm0.2</u>	<u>57.3\pm0.0</u>	91.9 \pm 0.0	<u>89.7\pm0.8</u>	<u>85.8\pm0.5</u>	<u>97.7\pm0.4</u>	43.2\pm0.4	92.5 \pm 0.1

Full-shot anomaly detection. We also investigate the upper bound of our method when all normal samples are utilized for anomaly generation and training. Table 2 presents the comparison results between ours and other full-shot methods, including UniAD [4], SimpleNet [34], DiAD [35], and AnomalyGPT [16]. It is evident that our method surpasses other alternatives by a large margin. Per-category results are listed in Table 12 and 13 in Appendix.

5.4 Ablation Study on Anomaly Detection

Influence of anomaly generation methods. To quantitatively compare with other anomaly generation methods, we train VLAD with anomalous samples generated by AnomalyDiffusion, DRAEM, NSA, and RealNet in the 1-shot setup and report the results in Table 3. The table indicates that anomalous samples generated by CUT yield the best detection results. Despite not being trained with anomalous samples from the test set, our anomaly detection results surpass those of AnomalyDiffusion in most metrics. This is notable given that AnomalyDiffusion has seen some of the test anomalous samples and thus introduced data leakage.

Influence of image/pixel-level supervisions. Table 4 presents the anomaly detection performance with different combinations of annotations. The results indicate that both image- and pixel-level annotations contribute to the final detection performance. Although CUT currently provides only coarse pixel-level annotations, these annotations offer valuable information, which can be effectively exploited with our proposed adapted Dice loss.

6 Conclusion and Future Works

In this paper, we propose CUT, a controllable, universal, and training-free visual anomaly generation framework that enables users to generate realistic anomalous samples from arbitrary normal images and anomaly descriptions. Within this framework, we introduce a novel mask-guided attention optimization strategy along with a localization-aware scheduler to address the limitations of SD in anomaly generation. Our approach achieves more authentic generation results without additional training compared to existing methods. Additionally, we propose an adapted dice loss that facilitates robust training on our generated anomalous samples with image-level and coarse pixel-level annotations, enhancing CUT’s effectiveness in downstream AD tasks. Extensive experimental results demonstrate the effectiveness of our proposed method.

Currently, CUT generates only coarse pixel-level annotations extracted from the attention maps. Our future work will focus on developing better approaches for acquiring higher-quality annotations. By generating fine-grained and diverse anomalies, CUT has the potential to contribute significantly to the development of foundational models for anomaly detection.

References

- [1] Yunkang Cao, Xiaohao Xu, Jiangning Zhang, Yuqi Cheng, Xiaonan Huang, Guansong Pang, and Weiming Shen. A survey on visual anomaly detection: Challenge, approach, and prospect. *arXiv preprint arXiv:2401.16402*, 2024.
- [2] Paul Bergmann, Kilian Batzner, Michael Fauser, David Sattlegger, and Carsten Steger. The MVTec anomaly detection dataset: A comprehensive real-world dataset for unsupervised anomaly detection. *International Journal of Computer Vision*, 129(4):1038–1059, 2021.
- [3] Chaoqin Huang, Aofan Jiang, Jinghao Feng, Ya Zhang, Xinchao Wang, and Yanfeng Wang. Adapting visual-language models for generalizable anomaly detection in medical images. In *IEEE/CVF Conference on Computer Vision and Pattern Recognition*, 2024.
- [4] Zhiyuan You, Lei Cui, Yujun Shen, Kai Yang, Xin Lu, Yu Zheng, and Xinyi Le. A unified model for multi-class anomaly detection. In *Advances in Neural Information Processing Systems*, pages 4571–4584, 2022.
- [5] Ruiying Lu, YuJie Wu, Long Tian, Dongsheng Wang, Bo Chen, Xiyang Liu, and Ruimin Hu. Hierarchical vector quantized transformer for multi-class unsupervised anomaly detection. In A. Oh, T. Naumann, A. Globerson, K. Saenko, M. Hardt, and S. Levine, editors, *Advances in Neural Information Processing Systems*, volume 36, pages 8487–8500, 2023.
- [6] Zheng Fang, Xiaoyang Wang, Haocheng Li, Jiejie Liu, Qiguai Hu, and Jimin Xiao. Fastrecon: Few-shot industrial anomaly detection via fast feature reconstruction. In *Proceedings of the IEEE/CVF International Conference on Computer Vision*, pages 17481–17490, 2023.
- [7] Vitjan Zavrtanik, Matej Kristan, and Danijel Skočaj. Draem-a discriminatively trained reconstruction embedding for surface anomaly detection. In *Proceedings of the IEEE/CVF International Conference on Computer Vision*, pages 8330–8339, 2021.
- [8] Ximiao Zhang, Min Xu, and Xiuzhuang Zhou. Realnet: A feature selection network with realistic synthetic anomaly for anomaly detection. In *IEEE/CVF Conference on Computer Vision and Pattern Recognition (CVPR)*, 2024.
- [9] Teng Hu, Jiangning Zhang, Ran Yi, Yuzhen Du, Xu Chen, Liang Liu, Yabiao Wang, and Chengjie Wang. Anomalydiffusion: Few-shot anomaly image generation with diffusion model. In *Proceedings of the AAAI Conference on Artificial Intelligence*, volume 38, pages 8526–8534, 2024.
- [10] Robin Rombach, Andreas Blattmann, Dominik Lorenz, Patrick Esser, and Björn Ommer. High-resolution image synthesis with latent diffusion models. In *Proceedings of the IEEE/CVF conference on computer vision and pattern recognition*, pages 10684–10695, 2022.
- [11] Hanqiu Deng and Xingyu Li. Anomaly detection via reverse distillation from one-class embedding. In *IEEE/CVF Conference on Computer Vision and Pattern Recognition*, pages 9737–9746, 2022.
- [12] Yunkang Cao, Xiaohao Xu, Zhaoge Liu, and Weiming Shen. Collaborative discrepancy optimization for reliable image anomaly localization. *IEEE Transactions on Industrial Informatics*, pages 1–10, 2023.
- [13] Karsten Roth, Latha Pemula, Joaquin Zepeda, Bernhard Schölkopf, Thomas Brox, and Peter Gehler. Towards total recall in industrial anomaly detection. In *IEEE/CVF Conference on Computer Vision and Pattern Recognition*, pages 14318–14328, 2022.
- [14] Alec Radford, Jong Wook Kim, Chris Hallacy, Aditya Ramesh, Gabriel Goh, Sandhini Agarwal, Girish Sastry, Amanda Askell, Pamela Mishkin, Jack Clark, et al. Learning transferable visual models from natural language supervision. In *International Conference on Machine Learning*, pages 8748–8763, 2021.
- [15] Jongheon Jeong, Yang Zou, Taewan Kim, Dongqing Zhang, Avinash Ravichandran, and Onkar Dabeer. Winclip: Zero-/few-shot anomaly classification and segmentation. In *IEEE/CVF Conference on Computer Vision and Pattern Recognition (CVPR)*, pages 19606–19616, 2023.
- [16] Zhaopeng Gu, Bingke Zhu, Guibo Zhu, Yingying Chen, Ming Tang, and Jinqiao Wang. Anomalygpt: Detecting industrial anomalies using large vision-language models. In *Proceedings of the AAAI Conference on Artificial Intelligence*, volume 38, pages 1932–1940, 2024.

[17] Xiaofan Li, Zhizhong Zhang, Xin Tan, Chengwei Chen, Yanyun Qu, Yuan Xie, and Lizhuang Ma. Promptad: Learning prompts with only normal samples for few-shot anomaly detection. In *Proceedings of the IEEE/CVF International Conference on Computer Vision*, 2024.

[18] Jake Snell, Kevin Swersky, and Richard Zemel. Prototypical networks for few-shot learning. *Advances in neural information processing systems*, 30, 2017.

[19] Dongyun Lin, Yanpeng Cao, Wenbin Zhu, and Yiqun Li. Few-shot defect segmentation leveraging abundant defect-free training samples through normal background regularization and crop-and-paste operation. In *2021 IEEE International Conference on Multimedia and Expo (ICME)*, pages 1–6. IEEE, 2021.

[20] Mircea Cimpoi, Subhransu Maji, Iasonas Kokkinos, Sammy Mohamed, and Andrea Vedaldi. Describing textures in the wild. In *Proceedings of the IEEE conference on computer vision and pattern recognition*, pages 3606–3613, 2014.

[21] Chun-Liang Li, Kihyuk Sohn, Jinsung Yoon, and Tomas Pfister. Cutpaste: Self-supervised learning for anomaly detection and localization. In *Proceedings of the IEEE/CVF conference on computer vision and pattern recognition*, pages 9664–9674, 2021.

[22] Hannah M Schlueter, Jeremy Tan, Benjamin Hou, and Bernhard Kainz. Natural synthetic anomalies for self-supervised anomaly detection and localization. In *European Conference on Computer Vision*, pages 474–489. Springer, 2022.

[23] Gongjie Zhang, Kaiwen Cui, Tzu-Yi Hung, and Shijian Lu. Defect-gan: High-fidelity defect synthesis for automated defect inspection. In *Proceedings of the IEEE/CVF Winter Conference on Applications of Computer Vision*, pages 2524–2534, 2021.

[24] Yuxuan Duan, Yan Hong, Li Niu, and Liqing Zhang. Few-shot defect image generation via defect-aware feature manipulation. In *Proceedings of the AAAI Conference on Artificial Intelligence*, volume 37, pages 571–578, 2023.

[25] Jie Hu, Yawen Huang, Yilin Lu, Guoyang Xie, Guannan Jiang, and Yefeng Zheng. Anomalyfusion: Multi-modal anomaly synthesis with diffusion. *arXiv preprint arXiv:2404.19444*, 2024.

[26] Jonathan Ho, Ajay Jain, and Pieter Abbeel. Denoising diffusion probabilistic models. *Advances in neural information processing systems*, 33:6840–6851, 2020.

[27] Alec Radford, Jong Wook Kim, Chris Hallacy, Aditya Ramesh, Gabriel Goh, Sandhini Agarwal, Girish Sastry, Amanda Askell, Pamela Mishkin, Jack Clark, et al. Learning transferable visual models from natural language supervision. In *International conference on machine learning*, pages 8748–8763. PMLR, 2021.

[28] Hila Chefer, Yuval Alaluf, Yael Vinker, Lior Wolf, and Daniel Cohen-Or. Attend-and-excite: Attention-based semantic guidance for text-to-image diffusion models. *ACM Transactions on Graphics (TOG)*, 42(4):1–10, 2023.

[29] Tsung-Yi Lin, Priya Goyal, Ross Girshick, Kaiming He, and Piotr Dollár. Focal loss for dense object detection. In *Proceedings of the IEEE international conference on computer vision*, pages 2980–2988, 2017.

[30] Carole H Sudre, Wenqi Li, Tom Vercauteren, Sébastien Ourselin, and M Jorge Cardoso. Generalised dice overlap as a deep learning loss function for highly unbalanced segmentations. In *Deep Learning in Medical Image Analysis and Multimodal Learning for Clinical Decision Support: Third International Workshop, DLMIA 2017, and 7th International Workshop, ML-CDS 2017, Held in Conjunction with MICCAI 2017, Québec City, QC, Canada, September 14, Proceedings 3*, pages 240–248. Springer, 2017.

[31] Paul Bergmann, Michael Fauser, David Sattlegger, and Carsten Steger. Mvtex ad—a comprehensive real-world dataset for unsupervised anomaly detection. In *Proceedings of the IEEE/CVF conference on computer vision and pattern recognition*, pages 9592–9600, 2019.

[32] Yang Zou, Jongheon Jeong, Latha Pemula, Dongqing Zhang, and Onkar Dabeer. Spot-the-difference self-supervised pre-training for anomaly detection and segmentation. In *European Conference on Computer Vision*, pages 392–408. Springer, 2022.

[33] Thomas Defard, Aleksandr Setkov, Angelique Loesch, and Romaric Audigier. Padim: a patch distribution modeling framework for anomaly detection and localization. In *International Conference on Pattern Recognition*, pages 475–489. Springer, 2021.

- [34] Zhikang Liu, Yiming Zhou, Yuansheng Xu, and Zilei Wang. Simplenet: A simple network for image anomaly detection and localization. In *Proceedings of the IEEE/CVF Conference on Computer Vision and Pattern Recognition*, pages 20402–20411, 2023.
- [35] Haoyang He, Jiangning Zhang, Hongxu Chen, Xuhai Chen, Zhishan Li, Xu Chen, Yabiao Wang, Chengjie Wang, and Lei Xie. Diad: A diffusion-based framework for multi-class anomaly detection. In *Proceedings of the AAAI Conference on Artificial Intelligence*, 2024.

A Appendix / supplemental material

A.1 More Implementation Details

For our proposed CUT, we set the inference steps to 200 with SD. For optimization, we set $\lambda = 10$ and Δt to $1.0/T$. As implemented in [28], the maximum value threshold to stop the iterative optimization at one time step t is set to 0.05, 0.5, 0.8, increasing with the denoising diffusion process. We apply our early-stopping strategy after the first 10 denoising steps and stop the optimization when $10 < n_t < 50$.

For VLAD, the images are resized to 512×512 for training. We train the VLAD model for 200 epochs with batch size 16. We use Adam optimizer with a learning rate of 1e4 and the CosineAnnealingLR scheduler. All experiments are run on a single NVIDIA A100-SXM4-80GB GPU.

A.2 More Details on VLAD Framework

Our proposed VLAD extends the work in AnomalyGPT [16], adapting CLIP [14] to compute the vision-language and vision-vision similarities and aggregates these similarities for anomaly detection.

Vision-Language Similarity The similarity between visual tokens and text embeddings for normal/anomalous states can indicate the abnormal level of visual tokens [15]. Specifically, for a given image, we first extract its patch tokens $\mathbf{F}_{patch}^i \in \mathbb{R}^{H_i \times W_i \times C_i}$ and image token $\mathbf{F}_{image} \in \mathbb{R}^{1 \times C}$ using the CLIP visual encoder, where i indicates the tokens that are extracted from the i -th stage of the image encoder. Then, text embeddings $\mathbf{F}_{text} \in \mathbb{R}^{2 \times C}$ representing normal/abnormal states are extracted via the CLIP text encoder. Since the extracted patch tokens have not undergone the final image-text alignment and cannot be directly compared with text features, we use a lightweight feature adapter comprising only a linear layer to project patch tokens for both fine-tuning and dimension alignment between visual and text embeddings, producing $\hat{\mathbf{F}}_{patch}^i \in \mathbb{R}^{H_i \times W_i \times C}$. The detection and localization results based on vision-language similarity can then be obtained as follows:

$$S_{VL} = \text{softmax}(\mathbf{F}_{image} \cdot \mathbf{F}_{text}^T), \quad M_{VL} = \text{Upsample} \left(\sum_{i \in \mathcal{H}} \text{softmax}(\hat{\mathbf{F}}_{patch}^i \cdot \mathbf{F}_{text}^T) \right) \quad (8)$$

where \mathcal{H} is the list of selected stages, and S_{VL} and M_{VL} denote the image- and pixel-level anomaly scores, respectively.

Vision-Vision Similarity When some normal samples are available, we utilize the same visual encoder and feature adapter to extract multi-hierarchy normal patch tokens and store them in memory banks $\mathbf{B}^i \in \mathbb{R}^{N_i \times C}$. Then, for the testing patch tokens, we compute the distance between each token and its most similar counterpart in the memory bank, and the localization result M_{VV} based on vision-vision similarities is yielded as follows:

$$M_{VV} = \text{Upsample} \left(\sum_{i \in \mathcal{H}} (1 - \max(\hat{\mathbf{F}}_{patch}^i \cdot (\mathbf{B}^i)^T)) \right) \quad (9)$$

The maximum value of M_{VV} is taken as the image-level anomaly scores S_{VV} . The predictions from vision-language and vision-vision similarities are summed up as final predictions.

A.3 User Study on Anomaly Generation Quality

To better assess the quality of our generated anomalous samples, we conducted a user study with 20 participants. The participants were shown exemplar normal samples of the five tested categories and asked to choose the most realistic anomalous images. We provided the participants with two groups of samples, as shown in Figure 9. In group 1, we randomly sampled three images each from 100 anomalous samples generated by Cut&Paste, DRAEM, NSA, AnomalyDiffusion, and our proposed CUT. Participants were asked to choose the three most realistic images for each category. For this group, we get a total vote of 300: $20(\text{participants}) \cdot 5(\text{categories}) \cdot 3(\text{selected samples per category})$. In group 2, we randomly sampled two images each from real anomalies in the test set and

from the 100 images generated by our method. Participants were then asked to choose the two most realistic images for each category. For this group, we get a total vote of 200: $20(\text{participants}) \cdot 5(\text{categories}) \cdot 2(\text{selected samples per category})$. The survey results are reported in Table 5 where we show the total votes from the 20 participants for each group. It is evident that our method surpasses other anomaly generation methods in terms of authenticity, even compared to AnomalyDiffusion, which leverages real test samples for training. Additionally, when mixed with real normal samples, our generated anomalous images are realistic enough to be misclassified.

Table 5: Results of user study for anomaly generation quality assessment across two groups.

Group 1					Group 2	
Cut&Paste	DRAEM	NSA	AnomalyDiffusion	Ours	Real	Ours
6	33	61	64	136	99	101

A.4 Per-category Anomaly Detection Results

In this section, we provide per-category anomaly detection results on MVTec and VisA. Few-shot detection results can be found in Table 6 to Table 11, and full-shot detection results are listed in Table 12 and Table 13.

A.5 More Anomaly Generation Results

More comparisons of anomaly generation results between other anomaly generation methods and CUT are provided in Figure 10. Additionally, to show the generalization ability and controllability of CUT, Figure 11 and 12 show more generation results with different object types and anomaly types.

A.6 More Anomaly Detection Results

More anomaly detection results are provided in Figure 13.

Table 6: Per-category anomaly detection performance on MVTec AD in the 1-shot setup. We report the mean and standard deviation over 5 random seeds for each measurement.

Category	I-AUC	I-F1	P-AUC	P-F1	PRO
bottle	98.9 \pm 0.1	97.9 \pm 0.5	96.3 \pm 0.0	71.0 \pm 0.2	92.7 \pm 0.0
cable	89.1 \pm 7.6	87.8 \pm 4.5	91.7 \pm 0.0	36.4 \pm 2.2	82.8 \pm 0.2
capsule	93.8 \pm 1.6	94.4 \pm 0.5	97.3 \pm 0.0	44.8 \pm 0.0	96.2 \pm 0.0
carpet	100.0 \pm 0.0	100.0 \pm 0.0	99.0 \pm 0.0	75.1 \pm 0.1	97.5 \pm 0.0
grid	97.3 \pm 1.3	96.1 \pm 2.2	97.2 \pm 0.0	49.8 \pm 0.1	92.0 \pm 0.1
hazelnut	99.9 \pm 0.0	99.3 \pm 0.2	98.4 \pm 0.0	63.5 \pm 0.1	97.3 \pm 0.0
leather	100.0 \pm 0.0	100.0 \pm 0.0	99.7 \pm 0.0	62.2 \pm 0.2	99.5 \pm 0.0
metal_nut	95.6 \pm 9.3	95.3 \pm 4.3	91.6 \pm 0.1	58.8 \pm 0.5	90.7 \pm 0.0
pill	93.7 \pm 0.4	96.0 \pm 0.1	94.3 \pm 0.0	56.6 \pm 0.2	97.0 \pm 0.0
screw	74.9 \pm 3.1	87.2 \pm 1.3	97.8 \pm 0.0	42.5 \pm 0.3	92.3 \pm 0.0
tile	99.6 \pm 0.0	98.8 \pm 0.2	95.6 \pm 0.0	73.2 \pm 0.0	93.3 \pm 0.0
toothbrush	94.1 \pm 2.7	93.1 \pm 5.6	98.5 \pm 0.0	56.6 \pm 1.3	94.7 \pm 0.0
transistor	91.4 \pm 2.1	80.7 \pm 4.4	79.6 \pm 0.0	37.1 \pm 0.2	64.0 \pm 0.2
wood	99.6 \pm 0.0	98.5 \pm 0.1	96.6 \pm 0.0	70.0 \pm 0.0	96.8 \pm 0.0
zipper	96.4 \pm 0.8	96.1 \pm 0.4	97.4 \pm 0.0	61.4 \pm 0.4	91.4 \pm 0.0
Average	94.9 \pm 0.4	94.7 \pm 0.4	95.4 \pm 0.2	57.3 \pm 0.0	91.9 \pm 0.0

Table 7: Per-category anomaly detection performance on MVTec AD in the 2-shot setup. We report the mean and standard deviation over 5 random seeds for each measurement.

Category	I-AUC	I-F1	P-AUC	P-F1	PRO
bottle	99.5 \pm 0.1	98.6 \pm 0.1	93.2 \pm 0.1	62.3 \pm 1.8	88.7 \pm 0.4
cable	89.3 \pm 1.4	86.5 \pm 2.0	94.9 \pm 0.0	41.1 \pm 0.8	86.0 \pm 0.3
capsule	95.1 \pm 1.1	94.6 \pm 0.9	96.6 \pm 0.2	44.9 \pm 0.0	96.1 \pm 0.1
carpet	100.0 \pm 0.0	100.0 \pm 0.0	99.3 \pm 0.0	76.5 \pm 0.1	98.1 \pm 0.0
grid	95.4 \pm 1.2	93.5 \pm 1.9	98.2 \pm 0.0	52.2 \pm 0.2	93.9 \pm 0.0
hazelnut	99.8 \pm 0.0	98.9 \pm 0.1	98.0 \pm 0.0	57.4 \pm 0.3	96.9 \pm 0.0
leather	100.0 \pm 0.0	100.0 \pm 0.0	99.7 \pm 0.0	66.1 \pm 0.3	99.5 \pm 0.0
metal_nut	99.8 \pm 0.0	99.1 \pm 0.4	94.6 \pm 0.1	66.7 \pm 0.5	93.2 \pm 0.1
pill	96.4 \pm 0.8	96.8 \pm 0.3	94.8 \pm 0.0	59.0 \pm 0.3	96.9 \pm 0.0
screw	78.8 \pm 3.2	88.4 \pm 0.1	98.2 \pm 0.0	46.6 \pm 0.2	93.5 \pm 0.0
tile	100.0 \pm 0.0	99.9 \pm 0.1	97.1 \pm 0.0	74.5 \pm 0.0	94.8 \pm 0.0
toothbrush	93.4 \pm 0.9	93.1 \pm 0.1	98.7 \pm 0.0	59.5 \pm 1.0	94.3 \pm 0.0
transistor	88.9 \pm 2.0	82.5 \pm 4.1	85.1 \pm 0.2	41.2 \pm 0.0	67.6 \pm 0.7
wood	99.4 \pm 0.0	97.7 \pm 0.1	96.9 \pm 0.0	70.9 \pm 0.1	97.0 \pm 0.0
zipper	99.4 \pm 0.0	98.3 \pm 0.4	97.7 \pm 0.0	63.6 \pm 1.5	92.8 \pm 0.4
Average	95.8 \pm 0.1	95.2 \pm 0.2	96.0 \pm 0.2	58.8 \pm 0.2	92.6 \pm 0.1

Table 8: Per-category anomaly detection performance on MVTec AD in the 4-shot setup. We report the mean and standard deviation over 5 random seeds for each measurement.

Category	I-AUC	I-F1	P-AUC	P-F1	PRO
bottle	99.2 \pm 0.0	98.0 \pm 0.5	96.9 \pm 0.0	73.0 \pm 0.1	93.7 \pm 0.0
cable	90.6 \pm 0.8	87.1 \pm 3.1	93.7 \pm 0.0	43.4 \pm 0.9	86.6 \pm 0.1
capsule	96.4 \pm 0.4	95.8 \pm 0.2	98.1 \pm 0.0	46.9 \pm 0.1	97.3 \pm 0.0
carpet	100.0 \pm 0.0	100.0 \pm 0.0	99.2 \pm 0.0	75.7 \pm 0.0	97.8 \pm 0.0
grid	98.4 \pm 0.8	96.9 \pm 2.6	98.1 \pm 0.0	52.4 \pm 0.0	93.6 \pm 0.0
hazelnut	98.9 \pm 0.2	97.6 \pm 0.4	98.6 \pm 0.0	63.1 \pm 0.3	97.3 \pm 0.0
leather	100.0 \pm 0.0	100.0 \pm 0.0	99.7 \pm 0.0	63.2 \pm 0.2	99.4 \pm 0.0
metal_nut	99.3 \pm 0.3	98.4 \pm 0.4	93.2 \pm 0.0	64.7 \pm 0.1	92.8 \pm 0.0
pill	97.3 \pm 0.1	97.4 \pm 0.1	94.9 \pm 0.0	59.4 \pm 0.1	97.3 \pm 0.0
screw	85.5 \pm 0.1	88.6 \pm 0.1	98.3 \pm 0.0	49.0 \pm 0.3	93.6 \pm 0.0
tile	99.8 \pm 0.0	98.7 \pm 0.1	95.9 \pm 0.0	73.3 \pm 0.0	93.6 \pm 0.0
toothbrush	94.3 \pm 1.3	94.1 \pm 0.8	98.6 \pm 0.0	60.2 \pm 0.9	94.2 \pm 0.1
transistor	87.5 \pm 1.9	75.9 \pm 4.1	82.8 \pm 0.0	39.5 \pm 0.2	67.4 \pm 0.1
wood	99.5 \pm 0.0	97.9 \pm 0.2	96.5 \pm 0.0	69.6 \pm 0.0	96.7 \pm 0.0
zipper	98.8 \pm 0.1	98.5 \pm 0.2	97.9 \pm 0.0	64.5 \pm 0.1	93.2 \pm 0.0
Average	96.4 \pm 0.1	95.1 \pm 0.1	96.2 \pm 0.1	59.8 \pm 0.1	93.0 \pm 0.0

Table 9: Per-category anomaly detection performance on VisA in the 1-shot setup. We report the mean and standard deviation over 5 random seeds for each measurement.

Category	I-AUC	I-F1	P-AUC	P-F1	PRO
candle	90.8 \pm 0.3	85.3 \pm 0.7	98.9 \pm 0.0	37.6 \pm 0.1	98.0 \pm 0.0
capsules	91.1 \pm 2.6	88.5 \pm 0.4	98.2 \pm 0.0	47.9 \pm 2.0	94.2 \pm 0.1
cashew	88.9 \pm 16.6	88.9 \pm 5.1	96.6 \pm 0.1	59.3 \pm 0.9	95.6 \pm 0.0
chewinggum	97.4 \pm 0.1	95.2 \pm 0.3	99.6 \pm 0.0	77.1 \pm 0.2	92.6 \pm 0.1
fryum	96.2 \pm 0.9	94.7 \pm 0.8	95.4 \pm 0.0	40.8 \pm 0.1	92.2 \pm 0.0
macaroni1	86.6 \pm 5.2	79.6 \pm 5.9	99.7 \pm 0.0	30.1 \pm 0.8	96.2 \pm 0.1
macaroni2	79.2 \pm 2.1	73.0 \pm 1.2	98.4 \pm 0.0	28.3 \pm 1.0	90.5 \pm 0.7
pcb1	90.8 \pm 2.0	86.1 \pm 1.5	98.5 \pm 0.0	49.5 \pm 4.6	93.6 \pm 0.0
pcb2	84.3 \pm 4.1	78.1 \pm 4.7	96.2 \pm 0.0	30.8 \pm 0.4	83.7 \pm 0.0
pcb3	78.0 \pm 5.2	74.3 \pm 1.7	94.9 \pm 0.0	32.7 \pm 11.4	86.0 \pm 0.0
pcb4	96.8 \pm 1.0	92.4 \pm 3.7	96.9 \pm 0.0	36.1 \pm 0.3	90.2 \pm 0.3
pipe_fryum	96.4 \pm 0.6	93.1 \pm 2.3	98.5 \pm 0.0	47.7 \pm 0.1	97.6 \pm 0.0
Average	89.7 \pm 0.8	85.8 \pm 0.5	97.7 \pm 0.4	43.2 \pm 0.4	92.5 \pm 0.1

Table 10: Per-category anomaly detection performance on VisA in the 2-shot setup. We report the mean and standard deviation over 5 random seeds for each measurement.

Category	I-AUC	I-F1	P-AUC	P-F1	PRO
candle	90.5 \pm 0.5	84.4 \pm 0.9	98.9 \pm 0.0	39.0 \pm 0.1	98.0 \pm 0.0
capsules	94.5 \pm 1.1	91.0 \pm 1.1	98.3 \pm 0.0	49.3 \pm 0.5	94.5 \pm 0.2
cashew	90.7 \pm 0.7	89.5 \pm 0.2	97.0 \pm 0.0	59.6 \pm 0.1	95.9 \pm 0.0
chewinggum	97.6 \pm 0.2	95.2 \pm 0.5	99.5 \pm 0.0	76.5 \pm 0.3	92.4 \pm 0.0
fryum	97.0 \pm 0.1	95.0 \pm 0.2	96.1 \pm 0.0	44.9 \pm 0.1	92.6 \pm 0.1
macaroni1	89.6 \pm 0.1	82.4 \pm 0.6	99.7 \pm 0.0	29.3 \pm 0.3	96.3 \pm 0.0
macaroni2	77.4 \pm 19.9	72.7 \pm 6.9	98.4 \pm 0.0	28.3 \pm 0.4	88.8 \pm 0.0
pcb1	92.0 \pm 0.5	87.7 \pm 0.5	98.5 \pm 0.0	49.3 \pm 3.0	93.9 \pm 0.0
pcb2	86.7 \pm 2.0	80.2 \pm 2.0	96.8 \pm 0.0	34.5 \pm 1.9	84.5 \pm 0.1
pcb3	84.6 \pm 0.4	78.6 \pm 0.2	95.4 \pm 0.0	40.5 \pm 4.5	86.1 \pm 0.1
pcb4	97.0 \pm 0.2	93.2 \pm 0.2	97.1 \pm 0.0	35.9 \pm 0.2	91.1 \pm 0.2
pipe_fryum	97.9 \pm 0.0	95.2 \pm 0.9	98.7 \pm 0.0	51.2 \pm 0.1	97.6 \pm 0.0
Average	91.3 \pm 0.4	87.2 \pm 0.6	97.9 \pm 0.4	44.9 \pm 0.3	92.7 \pm 0.1

Table 11: Per-category anomaly detection performance on VisA in the 4-shot setup. We report the mean and standard deviation over 5 random seeds for each measurement.

Category	I-AUC	I-F1	P-AUC	P-F1	PRO
candle	92.8 \pm 0.3	86.1 \pm 0.9	99.0 \pm 0.0	39.8 \pm 0.1	98.3 \pm 0.0
capsules	94.7 \pm 0.9	91.6 \pm 2.3	98.4 \pm 0.0	50.5 \pm 0.3	94.6 \pm 0.1
cashew	89.9 \pm 13.4	89.5 \pm 5.2	97.1 \pm 0.0	62.6 \pm 0.3	95.8 \pm 0.0
chewinggum	97.2 \pm 0.3	95.1 \pm 0.1	99.5 \pm 0.0	75.8 \pm 0.4	92.5 \pm 0.3
fryum	96.4 \pm 1.1	93.7 \pm 1.2	96.3 \pm 0.0	46.2 \pm 0.1	93.1 \pm 0.0
macaroni1	89.3 \pm 2.0	82.2 \pm 2.8	99.7 \pm 0.0	29.0 \pm 2.2	96.8 \pm 0.0
macaroni2	79.8 \pm 16.4	74.7 \pm 8.8	98.7 \pm 0.0	29.0 \pm 0.5	90.9 \pm 0.1
pcb1	88.3 \pm 11.4	81.3 \pm 17.4	99.2 \pm 0.0	70.1 \pm 1.1	93.9 \pm 0.0
pcb2	87.8 \pm 1.0	80.5 \pm 1.9	97.1 \pm 0.0	35.7 \pm 0.6	85.7 \pm 0.1
pcb3	89.6 \pm 1.2	82.3 \pm 3.6	96.2 \pm 0.0	47.2 \pm 1.3	89.0 \pm 0.1
pcb4	97.1 \pm 0.6	93.0 \pm 2.3	97.5 \pm 0.0	36.9 \pm 0.0	92.6 \pm 0.1
pipe_fryum	97.3 \pm 1.7	94.9 \pm 1.2</td			

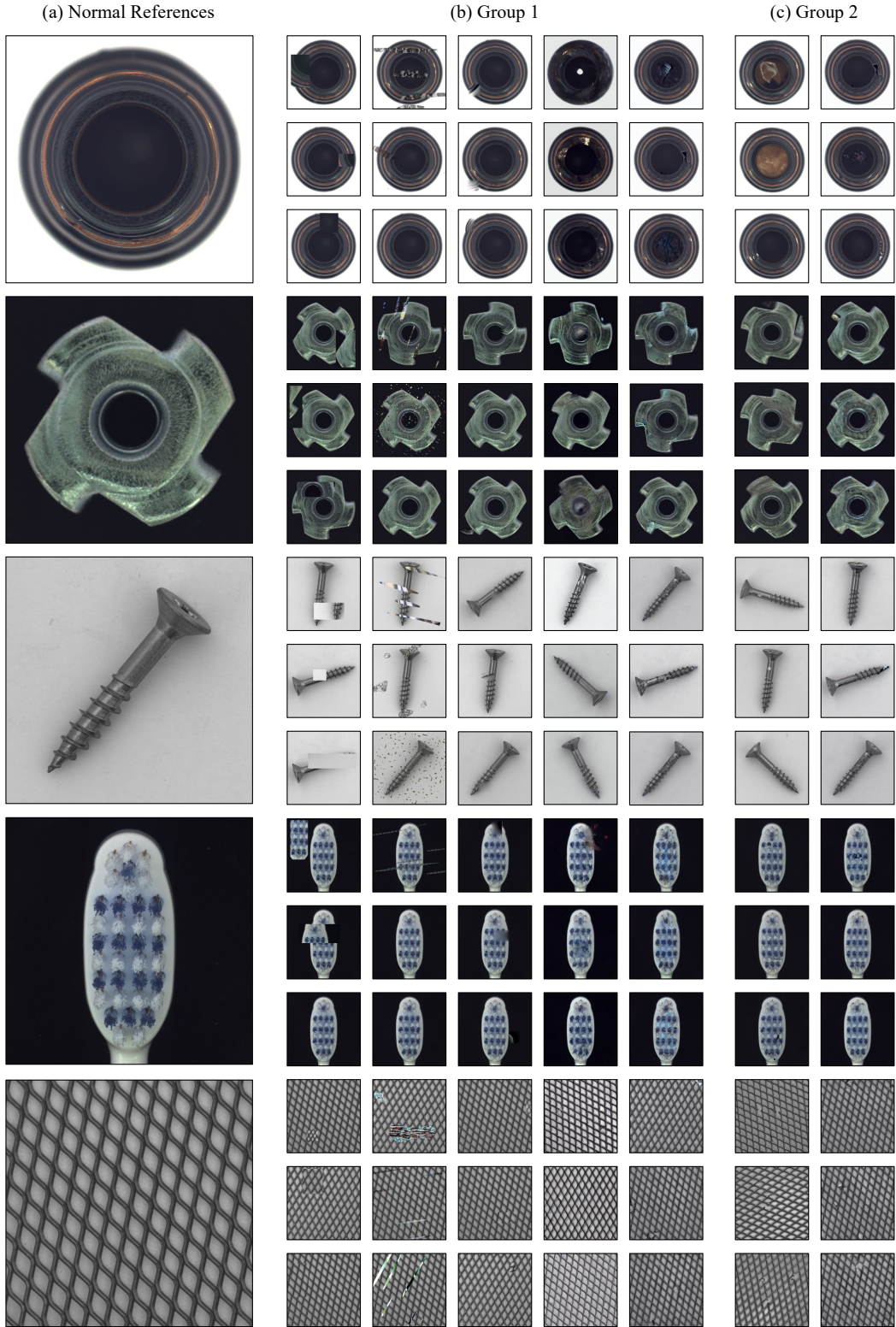


Figure 9: Samples for user study. (a) Normal references. (b) Group1: Samples of each column from left to right are generated by: Cut&Paste; DRAEM; NSA; AnomalyDiffusion; the proposed CUT ; (c) Group2: Samples of each column from left to right are real anomalous data samples from the dataset and anomalous images generated by our method CUT .

Table 12: Per-category anomaly detection performance on MVTec AD in the full-shot setup.

Category	I-AUC	I-F1	P-AUC	P-F1	PRO
bottle	99.7	98.4	97.5	74.9	94.7
cable	94.9	92.6	95.9	53.0	90.6
capsule	98.3	97.3	98.5	51.7	98.0
carpet	100.0	99.4	99.3	75.3	98.2
grid	99.8	99.1	99.1	52.7	96.6
hazelnut	99.7	98.6	99.4	76.3	98.5
leather	100.0	100.0	99.7	60.4	99.5
metal_nut	100.0	100.0	95.8	73.9	95.2
pill	98.5	98.3	96.3	63.6	97.9
screw	96.6	95.1	99.0	60.6	96.0
tile	100.0	99.4	97.2	74.6	94.8
toothbrush	96.9	95.2	99.5	71.5	97.8
transistor	94.3	84.2	88.0	45.2	70.0
wood	99.7	98.4	97.1	70.9	97.0
zipper	98.0	96.7	98.8	71.5	96.3
Average	98.4	96.9	97.4	65.1	94.7

Table 13: Per-category anomaly detection performance on VisA in the full-shot setup.

Category	I-AUC	I-F1	P-AUC	P-F1	PRO
candle	95.6	90.0	99.3	40.1	98.2
capsules	96.2	93.8	99.1	60.1	96.6
cashew	97.4	94.5	98.2	70.4	94.6
chewinggum	98.7	97.0	99.5	75.3	91.8
fryum	98.4	97.5	97.4	53.6	93.9
macaroni1	95.3	88.5	99.9	36.4	98.5
macaroni2	84.7	79.3	99.6	28.9	96.7
pcb1	95.9	91.8	98.8	41.8	95.4
pcb2	94.1	88.2	98.2	40.3	91.5
pcb3	95.9	90.4	97.5	52.9	93.4
pcb4	99.4	96.6	98.4	46.5	94.9
pipe_fryum	98.4	95.9	99.1	58.7	97.9
Average	95.8	91.9	98.7	50.4	95.3

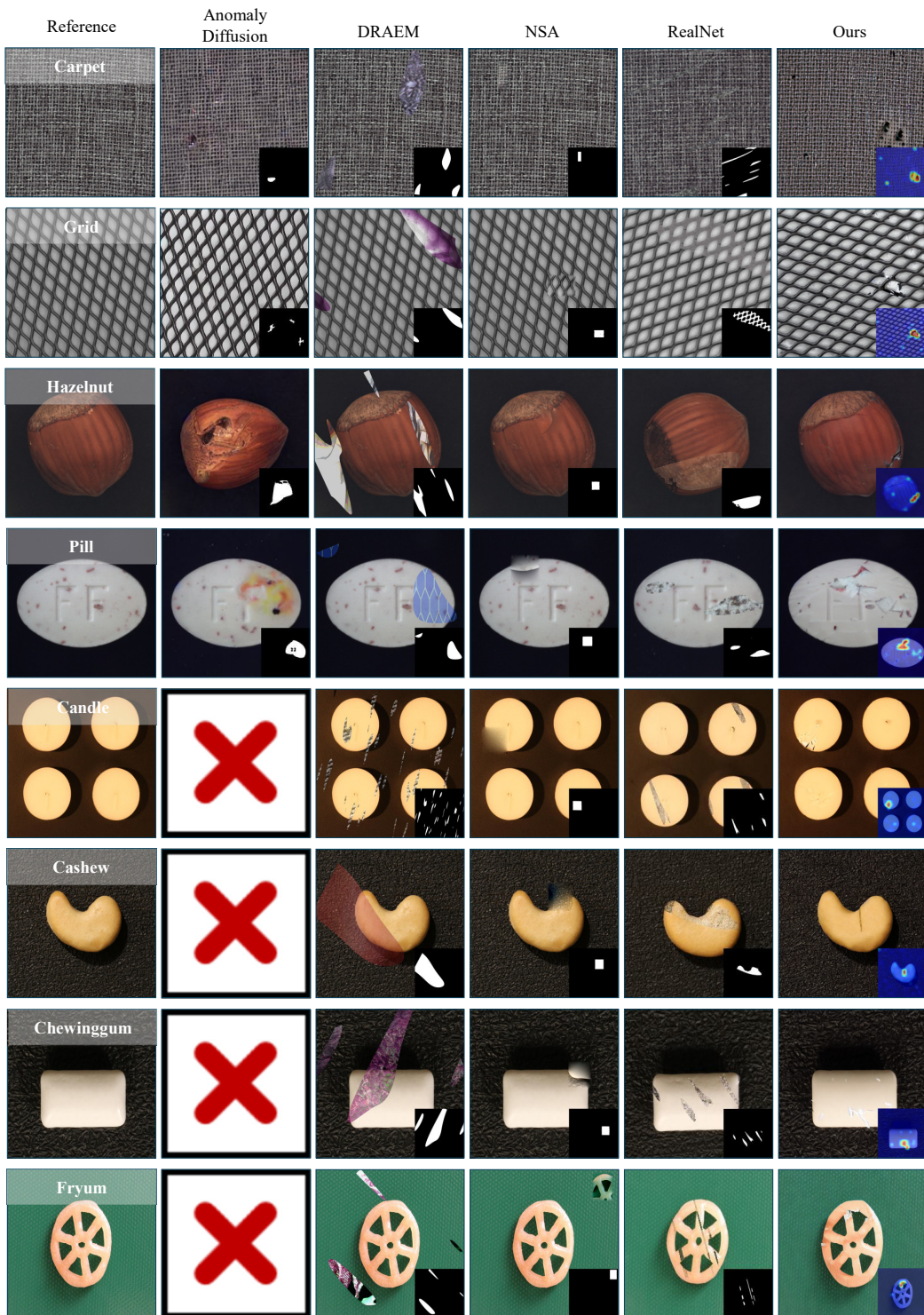


Figure 10: Qualitative comparisons between existing anomaly generation methods. Since Anomaly-Diffusion does not provide results on VisA, its corresponding generation results are replaced by a blank.

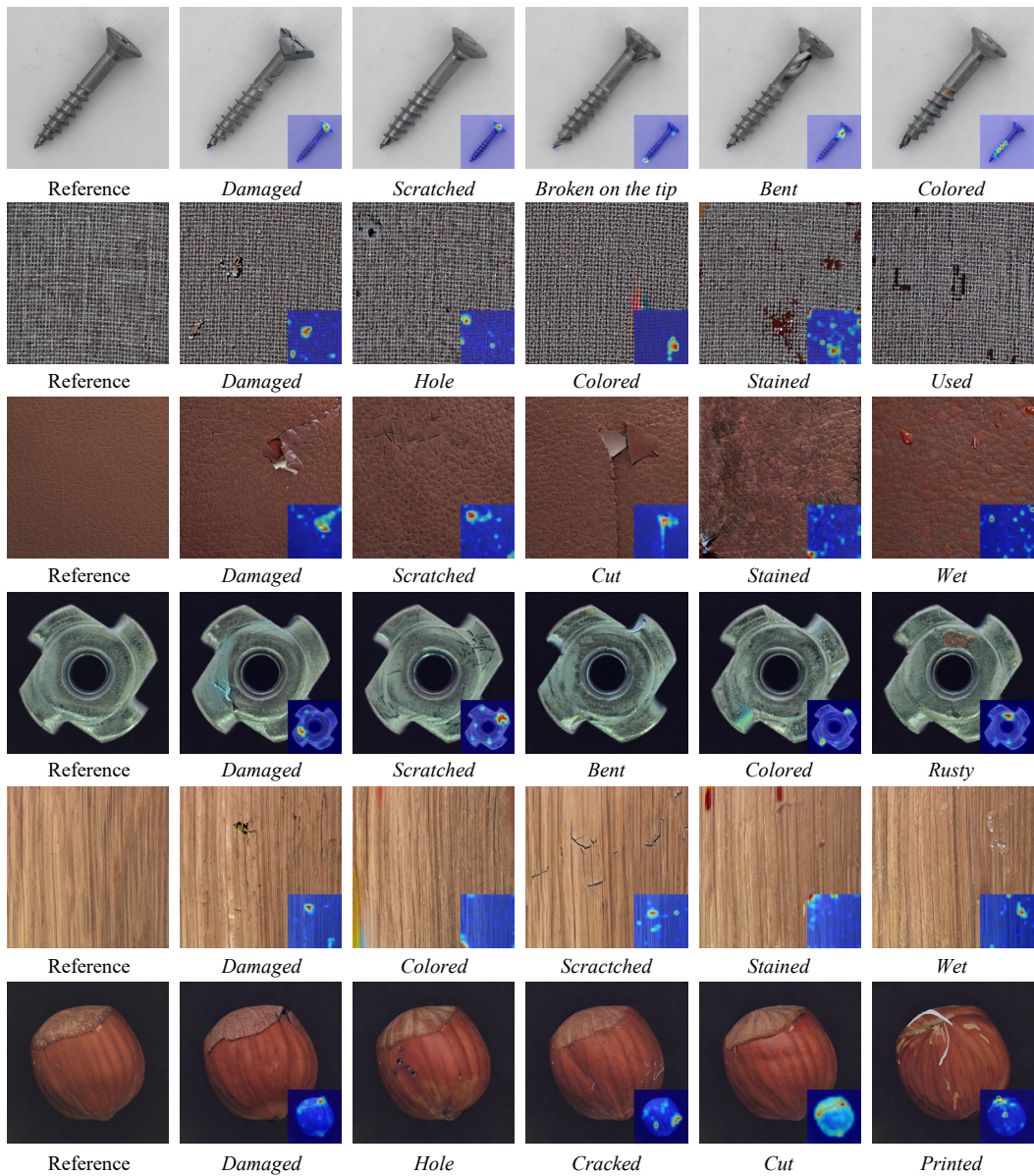


Figure 11: Anomaly generation results for arbitrary objects and anomaly descriptions.

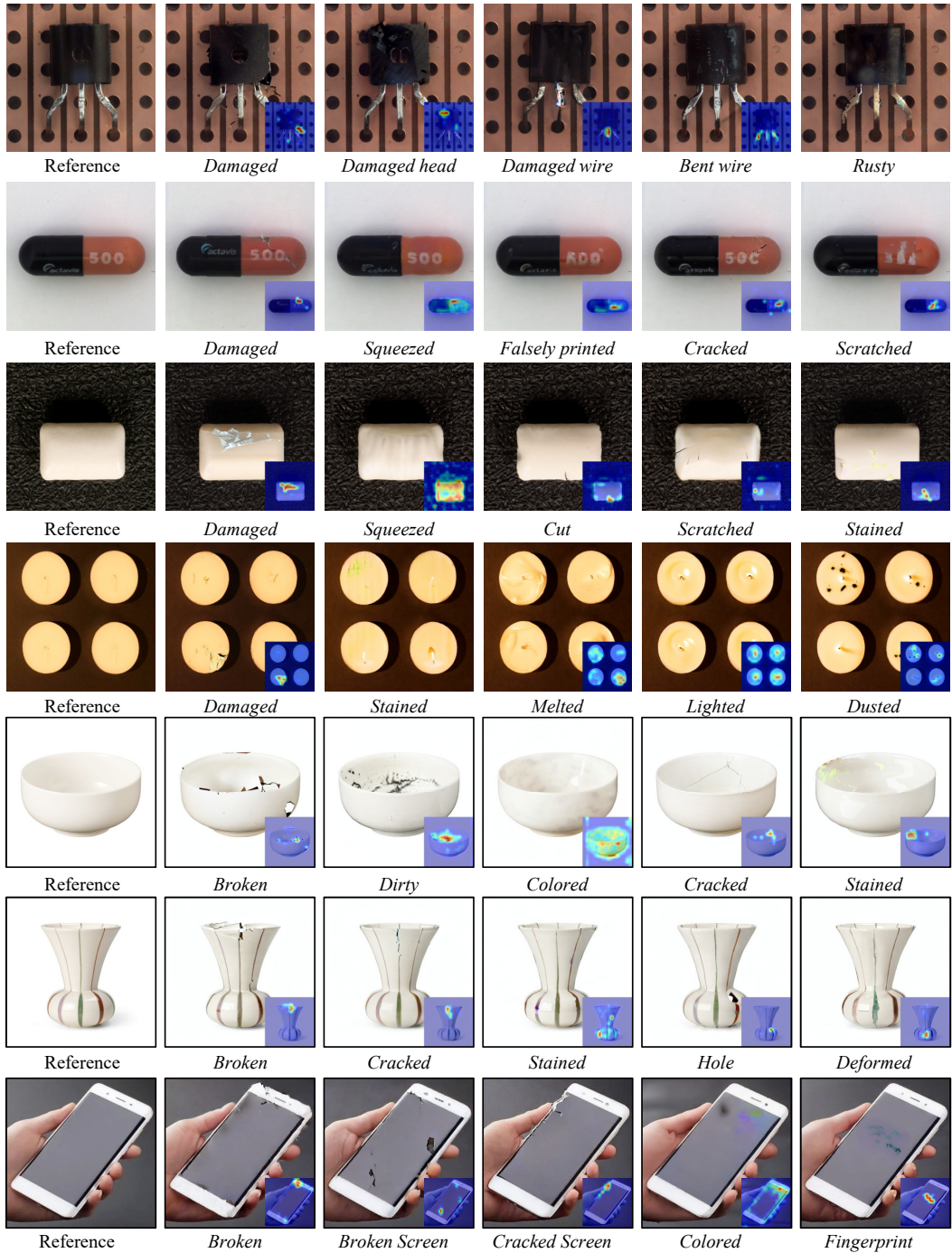


Figure 12: Anomaly generation results for arbitrary objects and anomaly descriptions.

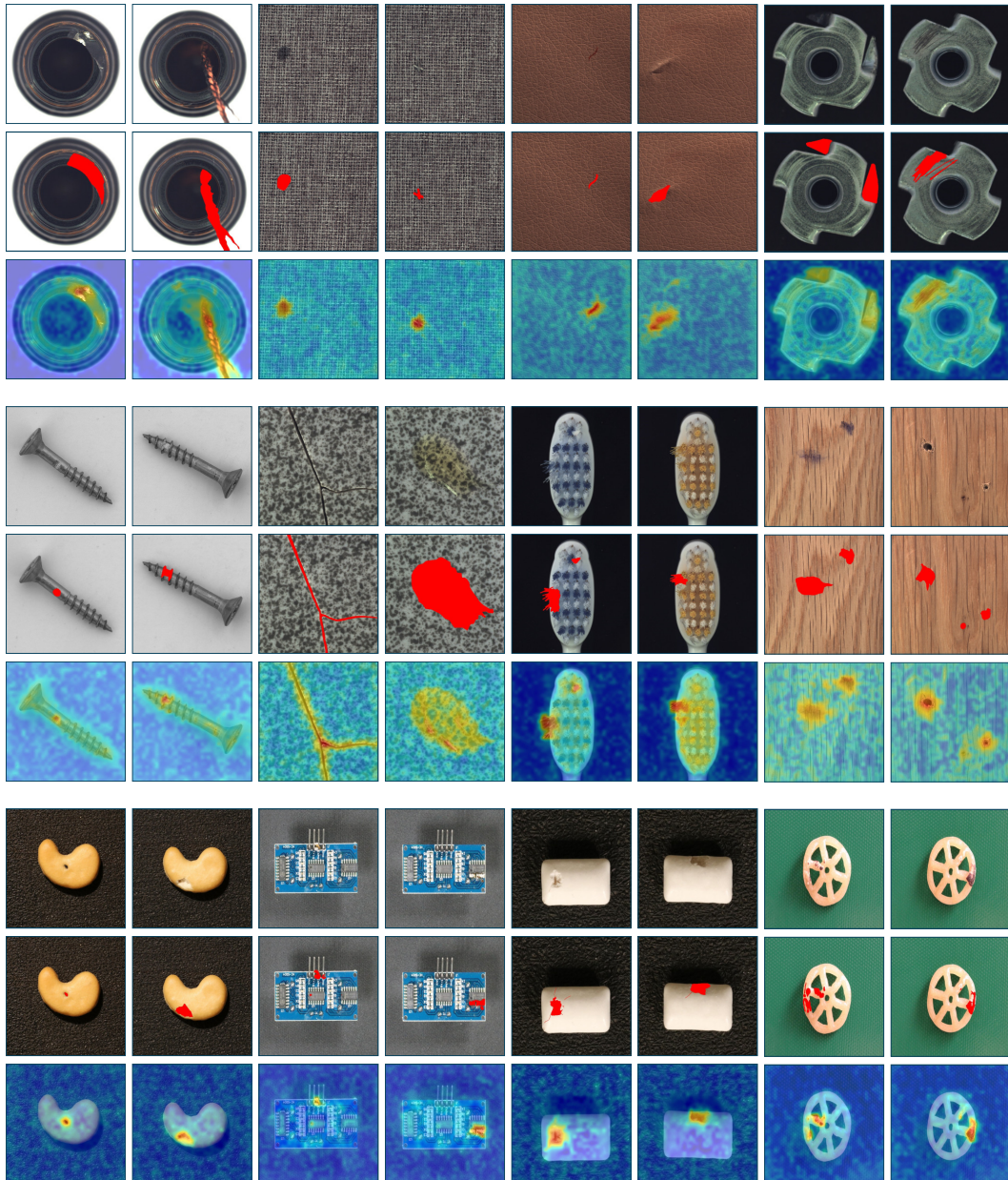


Figure 13: Anomaly detection results in the 4-shot setup. For each pair, the original image, ground truth, and detection results are listed from the top to the bottom.